



## Promoting microstructural homogeneity during flash sintering of ceramics through thermal management

Gareth M Jones, Mattia Biesuz, Wei Ji, Sandra Fisher John, Carolyn Grimley, Charles Manière, Claire E J Dancer

### ► To cite this version:

Gareth M Jones, Mattia Biesuz, Wei Ji, Sandra Fisher John, Carolyn Grimley, et al.. Promoting microstructural homogeneity during flash sintering of ceramics through thermal management. MRS Bulletin, 2021, 46 (1), pp.59 - 66. 10.1557/s43577-020-00010-2 . hal-03403730

**HAL Id: hal-03403730**

**<https://cnrs.hal.science/hal-03403730>**

Submitted on 27 Oct 2021

**HAL** is a multi-disciplinary open access archive for the deposit and dissemination of scientific research documents, whether they are published or not. The documents may come from teaching and research institutions in France or abroad, or from public or private research centers.

L'archive ouverte pluridisciplinaire **HAL**, est destinée au dépôt et à la diffusion de documents scientifiques de niveau recherche, publiés ou non, émanant des établissements d'enseignement et de recherche français ou étrangers, des laboratoires publics ou privés.

# Promoting microstructural homogeneity during flash sintering of ceramics through thermal management

Gareth M. Jones, Mattia Biesuz,\* Wei Ji,\* Sandra Fisher John, Carolyn Grimley, Charles Manière, Claire E.J. Dancer\*

Flash sintering (FS) is a novel field-assisted sintering technology, where the ceramic is heated internally by the Joule effect. While FS promises a tremendous reduction of ceramic firing time and furnace temperature, it has been applied only at the laboratory scale to date. The key limitation of scaling up the technique to the industrial manufacturing level is the intrinsic difficulty managing the heat generation and obtaining homogenous microstructures in components of industrial interest. Heterogeneous regions primarily originate from the different types of thermal gradients that develop during FS; therefore, the management of heat generation is crucial to achieve uniformity. In this article, we discuss the advantages of controlling the microstructural homogeneity of ceramics during FS, and the technical routes to achieve this. The origin and formation mechanisms of thermal gradients upon flash sintering are outlined. Possible approaches to reduce thermal and microstructural gradients are identified. The opportunities and challenges in scale-up of FS are discussed from both industrial and scientific perspectives.

## Introduction

The development of energy-efficient firing technologies has driven research on sintering throughout the twentieth century, with both economic and environmental motivations. Several novel low-energy consolidation techniques have been developed in the past decade, of which flash sintering (FS) is one of the most promising.<sup>1–3</sup>

FS is a field-assisted sintering technology where the simultaneous application of electric fields and heat to a ceramic green component leads to a sudden drop of its electrical resistivity, an internal heat generation by the Joule effect,<sup>4,5</sup> and densification within a few seconds. Attempts have been made to scale-up the flash process using other well-established sintering equipment such as flash-spark plasma sintering (flash-SPS)<sup>6–8</sup> and flash-microwave sintering,<sup>9,10</sup> though to date, the technique primarily remains at the laboratory scale.

In addition to reducing energy consumption, FS enables other enhancements to glass and ceramic manufacturing.<sup>11</sup>

The flash event can be used to facilitate the synthesis

of complex oxides,<sup>12</sup> formation of ceramic–ceramic<sup>13</sup> and metal–ceramic<sup>14,15</sup> joints, and viscous<sup>16</sup> and plastic<sup>17</sup> deformations. The flash event has also allowed the consolidation of microstructures<sup>18</sup> and phases<sup>19</sup> that cannot be achieved via conventional heating. Additionally, it has been shown to introduce a significant perturbation of the crystallographic and electronic defect chemistry.<sup>11,20,21</sup>

Several types of thermal gradient develop during FS as heat is internally generated by the Joule effect.<sup>4,5</sup> These gradients can occur over all length scales characteristic of the polycrystalline ceramics, from the macroscale bulk, to the microstructural features such as the grain size scale and the porosity scale, and the finest scales such as the grain-boundary and other interfaces.<sup>2</sup>

Such gradients can lead to undesired microstructural inhomogeneities in the sintered component. For the industrial adoption of FS in ceramic manufacturing, a key technological challenge is the fine control of current flow and hence heat transfer in the ceramic component during FS. In this article, different types of thermal gradients are

Gareth M. Jones, Warwick Manufacturing Group, University of Warwick, Coventry, UK; g.m.jones@warwick.ac.uk Mattia Biesuz, University of Trento, Trento, Italy; mattia.biesuz@unitn.it

Wei Ji, Wuhan University of Technology, Wuhan, China; jiwei@whut.edu.cn

Sandra Fisher John, Lucideon Ltd., Stoke-on-Trent, UK; sandra.fisher-john@lucideon.com Carolyn Grimley, Lucideon M+P, Greenville, USA; carolyn.grimley@lucideon.com

Charles Manière, Normandie Université, Caen, France; charles.maniere@ensicaen.fr

Claire E.J. Dancer, Warwick Manufacturing Group, University of Warwick, Coventry, UK; c.dancer@warwick.ac.uk

\*Corresponding authors

doi:10.1557/s43577-020-00010-2

described and their origins clarified. This is followed by a comprehensive discussion of solutions to avoid thermal and microstructural gradients.

## Temperature and microstructural heterogeneity

### Origin of microstructural inhomogeneities

FS experiments are often carried out on small specimens to minimize thermal heterogeneity. However, the use of samples of even a few millimeters in thickness has been reported to generate temperature heterogeneities<sup>3</sup> ranging over a few hundred degrees Celsius in some cases. Evidence of this comes from thermal images,<sup>22–24</sup> microstructural variations,<sup>25</sup> and X-ray diffraction peak width broadening.<sup>26</sup> The origins of the thermal gradients and their consequent microstructural inhomogeneities are indicated in Figure 1. We can outline two main categories of thermal gradient: in the sample cross section (i.e., orthogonal to the current flow) and along the gauge length (i.e., in the direction of the current flow). In the following sections, we expand on this categorization and discuss how they enable the development of different microstructural variations.

### Thermal inhomogeneities and gradients

Thermal gradients in the sample cross section upon FS arise

from a disparity between the rate of Joule heating in the sample and the rate of heat transfer and are initiated by surface

cooling fluxes. The negative temperature coefficient (NTC) resistivity of most ceramics implies a higher current concentration and thermal dissipation in the hot zones.<sup>4</sup> The developed surface-to-core temperature differences depend on the applied electric power, the thermal conductivity, the sample geometry, and the activation energy for electrical conductivity. This NTC phenomenon, combined with the specimen cooling at the boundaries, tends to amplify the temperature gradients and may generate highly unstable heating regions.<sup>27,28</sup> These so-called hot spots can be detected in samples after sintering through microstructural features, including local melting,<sup>3</sup> and abnormal grain growth.<sup>29</sup> Grain core-boundary temperature differences are minimal and unlikely to contribute significantly to the temperature gradients.<sup>30</sup>

Several researchers have modeled the heat distribution in the samples during FS.<sup>31–35</sup> Homogenous heat capacity and transfer are commonly assumed for the bulk material. These studies focus on macroscale effects over the whole sample or on nanoscale effects at particle–particle interfaces, with intermediate scales neglected. A simulation study by Dong based on perturbation methods tests the validity of this assumption and shows the hot spot phenomenon may be active for specimens above a certain critical size ( $Z_{cr}$ ) as low as a few millimeters for yttria-stabilized zirconia (YSZ):<sup>36</sup>

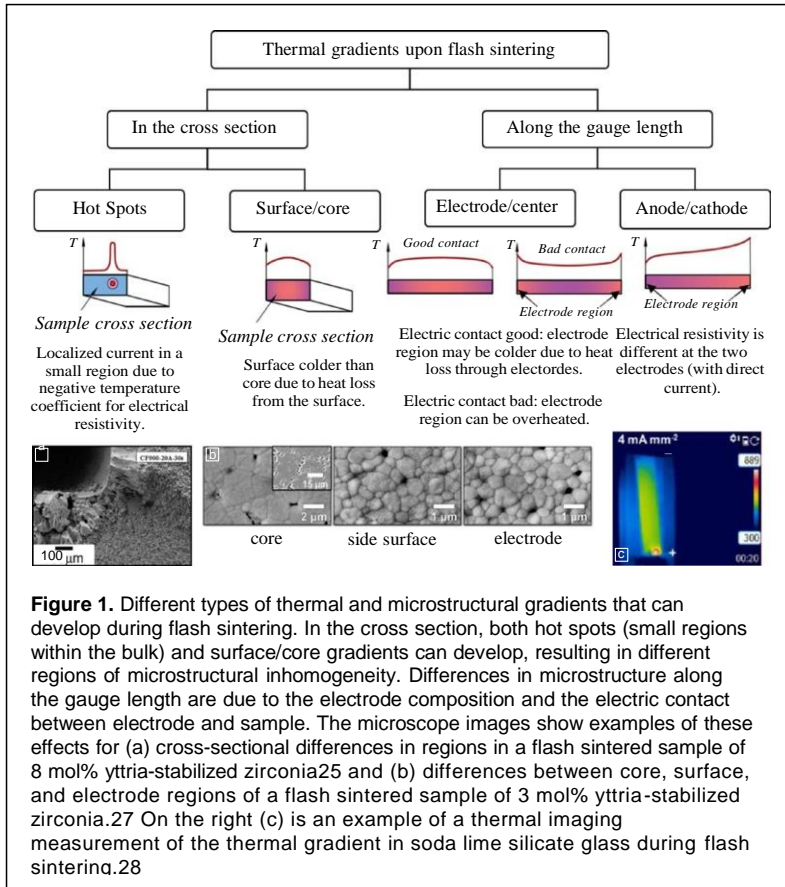
$$Z_{cr} = \frac{2\kappa(T)\rho(T)RT^2}{QE^2} = \frac{2kRT^2}{pQ}, \quad (1)$$

where  $\kappa(T)$  represents the thermal conductivity,  $\rho(T)$  represents the electrical resistivity,  $Q$  represents the corresponding activation energy,  $p$  represents the electric power density,  $R$  represents the gas constant,  $T$  represents the absolute temperature, and  $E$  represents the electrical field.

The existence of a critical hot spot size is due to the fact that the volumetric heat produced by a temperature perturbation increases with the square of the perturbation radius ( $\lambda$ ), whereas the heat dissipated toward the neighboring regions of the specimen is linear with  $\lambda$ . Thus, when  $\lambda > \lambda_{cr}$ , the volumetric heat is dominant and the perturbation is stable, on the other hand, if  $\lambda < \lambda_{cr}$  heat is exchanged with the surrounding and the perturbation vanishes. Additional thermal gradients could develop close to microstructural features such as grain boundaries<sup>2</sup> and pores.<sup>37</sup>

### Geometry and electrode contact effects

The geometry of the sample and attached electrodes has a significant effect on the development of thermal gradients during FS. The magnitude of a thermal gradient from surface to core depends primarily on the exposed surface area of the sample, power dissipated (both



dependent on geometry), and thermal conductivity (material property).

Small non-industrially relevant sample geometries such as dogbones have been extensively used in FS studies. Their minimized cross-sectional area reduces the severity of the gradient between the surface and core. For long gauge lengths, anode/cathode and electrode/core gradients are non-negligible. Field enhancement at the electrode hole can further enhance the thermal gradient.<sup>38</sup> Dogbones have typical gauge length of 15–20 mm with a cross-sectional area of 3–6 mm<sup>2</sup>.<sup>39–42</sup>

In the case of disk-shaped samples, which have a larger diameter compared to their height, the ratio between the area in contact with the electrodes and the curved side surface depends on the height-to-diameter ratio with heat dissipation through the electrodes becoming dominant in the case of thin samples. The small height minimizes any gradient between the sample center and the electrode region, but also facilitates the formation of hot spots and radial gradients.<sup>43</sup> Common sizes of disk vary, but most used in FS experiments are less than 10 mm in diameter,<sup>44–46</sup> the exception being flash-SPS where larger disk diameters are more common.<sup>47–51</sup> When “pellet” samples are used (i.e., cylindrical-shaped samples with similar diameter to height),<sup>27</sup> geometry effects lie between the two extremes of the dogbone (low diameter-to-height ratio) and the disk (high diameter-to-height ratio).

Poor contact of the sample to the electrode introduces high resistance in the electrode region over which power is dissipated. Overheating of the electrode region can produce excessive grain growth at both the anode and cathode for direct current (DC) and alternating current (AC).<sup>38</sup> Good thermal contact between the sample and electrodes allows heatsinking from the sample to cooler electrodes.<sup>27</sup>

### ***Material-dependent effects***

The bulk material properties affect thermal homogeneity through the thermal conductivity and the electrical resistivity (Equation 1).<sup>36</sup> The activation energy ( $Q$ ) for electrical conductivity in ceramics varies significantly and this affects the probability of hot spot formation. Hot spots become more stable in materials possessing high  $Q$  and low  $k$ , or when high power density is applied (Equation 1). The behavior of materials undergoing flash sintering depends on the relative values of their electrical and thermal conductivity. The presence of impurities, dopants, or secondary phases in ceramic composites can alter the electrical and thermal conductivity and hence the FS behavior. Composite materials can have complicating effects if the conductivity of the constituents varies as in alumina–titania<sup>52</sup> and alumina–zirconia composites.<sup>53</sup> Similar effects may occur when using reactive flash.<sup>54</sup> The presence or formation of thermally conductive phases during FS can act as a heatsink or thermal buffer to mitigate hot spot formation, such as the glass phase in porcelain.<sup>55</sup> The packing of the ceramic compact also affects the overall contact resistance and ease of FS, smaller particles pack better with a higher ratio of

particle–particle contact to surface area compared to larger particles.<sup>56</sup>

Electrochemical effects associated with the application of a DC electric potential have been observed during FS in several ceramic systems. These phenomena are particularly relevant in ionic conductors where the displacement of ions under the effect of the external field leads to variations in the sample composition between the anode (+) and cathode (–). In alkali-ion conductors, such as soda lime silicate glass, FS causes a substantial accumulation of the positive charge carriers at the cathode and a highly resistive alkali depletion layer forms at the anode.<sup>57,58</sup> The local increase in the electrical resistivity causes a substantial overheating of the anodic region (even  $> 1000^{\circ}\text{C}$ ), observed using thermal imaging.<sup>57,58</sup> Electrochemical phenomena have also been reported in oxygen ion conductors, including YSZ<sup>23,59</sup> and gadolinium-doped ceria.<sup>20,60,61</sup> Here, the mobile charge carriers are oxygen vacancies,  $\text{vO}$ , which move and accumulate at the cathode.

$\text{vO}$  accumulation is somewhat counterbalanced by molecular oxygen reduction from the atmosphere at the cathode, which acts as a partially blocking electrode.

The molecular oxygen reduction rate is highly dependent on the electrode configuration<sup>59</sup> and is often not sufficient to sustain the current flow. This leads to a strong electrochemical reduction of the cathodic region, which propagates to most of the gauge length during FS. This phenomenon is associated with visible electrochemical blackening<sup>62</sup> due to the formation of donor levels in the bandgap.<sup>23</sup> This anode/cathode asymmetry causes thermal gradients due to imbalance in the concentrations of positive and negative charge carriers, leading to overheating of the anode.<sup>23,24</sup> In addition to these thermal effects, cathodic electrochemical reduction induces microstructural gradients due to localized changes in the diffusivity of cations.<sup>63,64</sup> While the most extreme electrochemical effects have been observed in ionic conductors, anode/cathode asymmetry, reduction, or blackening has been reported during FS in several ceramic systems.<sup>11</sup>

### ***Microscale microstructural development***

While FS can cause the formation of large inhomogeneous regions on the scale of the sample that are clearly detrimental, on the microscale, it promotes significant homogeneity compared to other sintering techniques. Recently, Ji et al.<sup>65</sup> compared the microstructure of 3YSZ produced by different densification technologies: conventional sintering, fast firing, self-propagating high-temperature synthesis, and FS (Figure 2). By heating to different temperatures, both partially and fully dense materials were obtained using each technique. Conventionally sintered (Figure 2a–b) samples showed heterogeneous microstructures with pores of high coordination number originating from the green compact. Pores and abnormal grain growth were also observed in samples produced by fast firing (Figure 2c–d) and self-propagating high-temperature synthesis (Figure 2e–f). Large pores shrink proportionally to the macroscopic shrinkage of the body and are difficult to fully

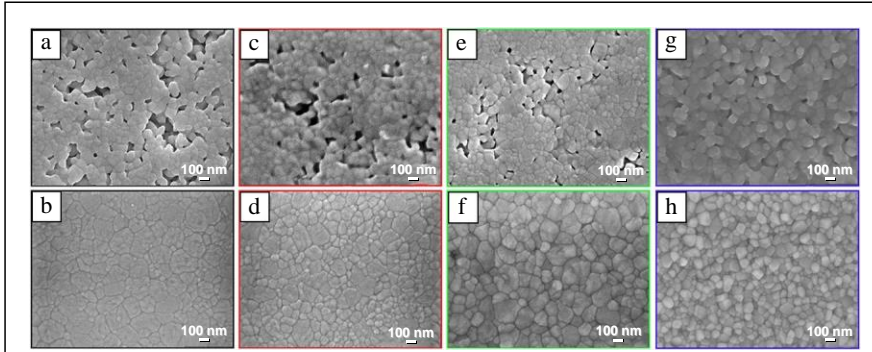


**Figure 2.** Morphology of partially and fully dense samples upon (a, b) conventional sintering, (c, d) fast firing, (e, f) self-propagating high-temperature synthesis, and (g, h) flash sintering<sup>65</sup>.

remove. In contrast, the partially dense FS specimen had a fine and uniform porosity, and the fully dense sample was homogeneous (Figure 2g–h). In the FS sample, only small pores with low pore coordination number were observed, demonstrating that FS accelerates the homogenization of the morphology in the microscale. This difference in pore size contributes significantly to the greater densification rate following rapid heating with or without an electric field.<sup>66</sup>

## Strategies to reduce temperature and microstructural gradients

### Modeling thermal gradients

Thermal gradient development is highly influenced by the cavity configuration in FS and can be most easily explored using finite element simulation.<sup>67</sup> “Hybrid” heating uses an additional external heat source to homogenize the thermal field. For “direct” heating of thick specimens, high-temperature differences are expected, even assuming a uniform volumetric dissipation (Figure 3a).<sup>36,67</sup> The relative cooling fluxes at the specimen boundaries are calculated as ~ 70% radiation, ~ 20% convection, and ~ 10% conduction for the configuration shown in Figure 3a at high temperature. The dominant radiative contribution is easily explained by the  $T^4$  Stefan–Boltzmann Law. Egorov et al.<sup>68</sup> state the convective relative cooling proportion may be higher if the heated specimen is immersed in a large air cavity.

Thermal gradients originating from cooling fluxes due to boundaries can be reduced by three main approaches:<sup>67</sup> first, by lowering the heating cavity air volume using thermal insulation; second, by delaying the cooling core/edge gradient development by imposing ultrarapid heating from the start (or using double-step or multistep FS); and third, by employing hybrid heating using a susceptor or an external heating element. As indicated by Figure 3c,

the most efficient way to reduce the thermal heterogeneities in direct heating is a configuration combining thermal insulation and high heating rate.<sup>67</sup> This conclusion is valid in both flash-microwave sintering and “standard” FS. A similar approach was applied to FS by thermally insulating the specimen using coarse zirconia powder or an alumina foil/wool. This approach increases the homogeneity of the microstructure while significantly reducing the energy consumption.<sup>69</sup>

In microwave sintering, a susceptor is used to homogenize and stabilize the heating.<sup>70</sup> Hybrid heating can also be applied to “traditional flash” and microwave flash experiments where the susceptor is electrically heated to follow the heating of the sample. This approach is commonly employed in flash-SPS, where a graphite foil/felt is used to activate the flash transition. This allows the production of specimens with large diameters (30–60 mm)<sup>7,49</sup> and homogeneous microstructures can be obtained. Simulation explains this stability by the lateral graphite elements heating (electrical susceptor) and thermal confinement originating from thermal contact resistance at each interface.<sup>8</sup>

## Experimental solutions

### Power delivery and heating rate

In this section, we discuss possible technical solutions to avoid or mitigate the effects of the formation of thermal gradients during FS.

As the hot spot critical size (Equation 1) decreases when increasing the applied power, the power peak at the voltage-to-current control switching facilitates hot spot formation and so has a detrimental effect on the final microstructure. One simple solution is to operate under a low current limit from the start. This “power-controlled” method results in a much

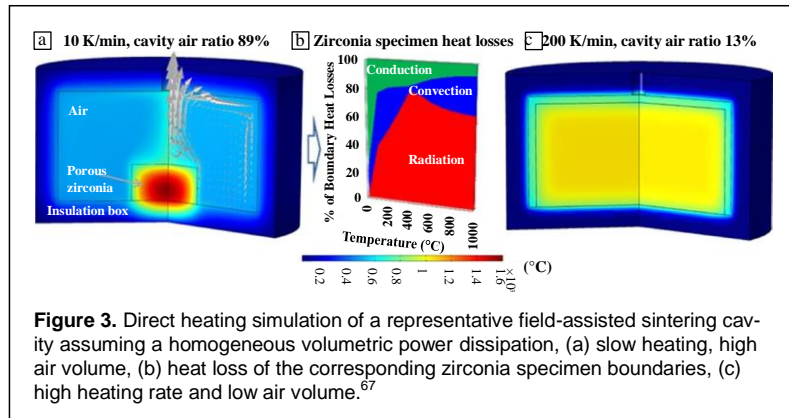


**Figure 3.** Direct heating simulation of a representative field-assisted sintering cavity assuming a homogeneous volumetric power dissipation, (a) slow heating, high air volume, (b) heat loss of the corresponding zirconia specimen boundaries, (c) high heating rate and low air volume.<sup>67</sup>

slower heating rate,<sup>71</sup> but limits the likelihood of hot spot formation. An alternative is to adapt the two-step conventional sintering process to FS.<sup>25,46</sup> The interruption in current flow reduces instances of current concentration, as when the flash is reinitiated the current will find a different unblocked path. Proportional integral derivative (PID) control produces current ramps with rates varying from 1 A/cm<sup>2</sup>/s to 0.001 A/cm<sup>2</sup>/s. At slow ramp rates, increased grain growth was observed.<sup>72</sup> Using a similar method, different ramp profiles (linear, square-root, and parabolic) were trialed.<sup>73</sup> Current limit stepping via PID has been built into FS protocols<sup>74</sup> and resulted in superior homogeneity between the surface and core.<sup>75</sup> The use of the current ramp FS approach also resulted in a smaller anode/cathode grain size difference in 3YSZ.<sup>41</sup>

To provide reproducibility and control required to adapt FS to industrial applications, Lucideon Ltd. has developed a control system based on a nonlinear algorithm. In conjunction with a real-time computer, the software controls current, voltage, or power outputs on a millisecond basis, preventing any value from overshooting its set point. Controlled ramps of any of the previously discussed parameters and pulsed power dissipation can be achieved, and the system functions at frequencies ranging from DC up to the megahertz range.<sup>76</sup>

### Electrode configurations

The electrode material and interface paste composition (if used) can greatly affect the contact resistance in FS. Several different electrode configurations have been proposed to solve or alleviate electrode effects. The effect of electrochemical redox under DC can be mitigated through the use of porous mesh electrodes and pastes<sup>59</sup> (i.e., electrodes that facilitate O<sub>2</sub> diffusion and its incorporation at the cathode). Another solution is the use of molten salt electrodes, which can supply ionic species to the depleted electrode region in alkali-ion conductors,<sup>28</sup> though the use of AC fields is more generally applicable.<sup>23,77</sup> The adoption of an optimized electrode shape<sup>78,79</sup> can also alter the thermal gradient. A solution to enable continuous production has been developed by a collaboration between the University of Colorado and Lucideon Ltd. using sliding electrodes above and below a whiteware sample within a rolling kiln.<sup>80</sup>

Contactless FS opens up opportunities for components with unfavorable geometries, including thin films for solid-oxide fuel cells and solid-state batteries, environmental and thermal barrier coatings, as well as complex geometries with non-uniform thickness. Contactless FS may avoid the formation of thermal gradients caused by electrode-specimen contact as it delivers current to the sample via a conductive gaseous medium between the electrode and the sample. Successful trials of contactless FS have used electric arcs, cold plasma, and local heating using an electrically conductive flame.<sup>81–83</sup> Lucideon Ltd. has developed a demonstration scale system for contactless flash sintering.<sup>76</sup> The system consists of a multiaxis robot capable of full dimensional rastering allowing homogeneous flash sintering of large areas and thin (< 1 mm)

geometries. The system has also been used for localized room-temperature repair of glaze defects on sanitary ware.

### Additives

From Dong's equation (Equation 1), at a given temperature, the critical size of a hot spot rises as the activation energy for electrical conductivity is reduced. This can be achieved by adding electrically conductive phases to the ceramic, including carbon nanotubes,<sup>84</sup> graphene,<sup>85–87</sup> or graphite.<sup>88</sup> The addition of these compounds also increases the overall thermal conductivity of the specimen, which further decreases the hot spot formation probability and reduces the surface/core thermal gradients. Preliminary results have also shown that the addition of water ("cold FS") allows flash of thin pellet-like samples at room temperature without hot spot formation.<sup>89</sup>

### Summary

We have described how a variety of thermal gradients form during flash sintering, leading to microstructural inhomogeneities. A range of strategies have been proposed to mitigate and manage this formation; these are summarized in **Table I**.

It is clear that the strategies chosen to implement FS on an industrial scale will be shaped by the requirements of each product and the benefits pursued by its manufacturer. For instance, small additions of a more conductive phase will lead to homogeneity improvement by mitigating the thermal gradient between the sample core and edges. At the same time, this tunes the optical and electrical properties of the final product, which may be detrimental for some applications. While it is unlikely that any single solution would be universally appropriate, some inhomogeneity mitigation strategies are more amenable to large-scale production.

Contactless FS offers the most extensive set of benefits, by removing the need for expensive electrode materials, mechanisms to ensure contact is maintained (conductive paste and/or uniaxial pressure), and the limitation to geometries, which possesses a regular cross section and provides two flat surfaces for contact. Currently, contactless has been successfully used for applications requiring thin ceramic layers, such as thermal barrier coatings.<sup>82</sup>

The next most practical solutions are the use of AC and electrical control systems. In the laboratory, uncontrolled DC is preferred due to its simplicity. For a manufacturer, any additional difficulty introduced by controlled AC is small compared to the overall cost of retrofitting a line for FS and is beneficial for stability and homogeneity. These two strategies can greatly reduce hot spot formation and electrochemical reduction effects.

Reducing the macroscopic thermal gradients induced by heat loss at free surfaces and electrodes is key to the adoption of FS as an industrial-scale technology. Continued work on the effect of alternate paste compositions and morphologies would aid in the development of flash for more specialized batch processes. However, continuous throughput processes are not readily amenable to the use of pastes or physical insulation. Thermal

**Table I. The origins of thermal gradients and strategies to mitigate their formation.**

Type of gradient	Origin	Materials	Strategies
Surface/core (core overheated with respect to surface)	Heat radiation from the hot surface	· Materials with low thermal conductivity	· Addition of a thermally conductive phase · Ultrafast (very small time scale)/pulsed · Decrease heating rate · Use of susceptor (hybrid heating) · Use of thermal insulation
Hot spot	Thermal instability related to the negative temperature coefficient for electrical resistivity	· Materials with low thermal conductivity · Materials with negative temperature coefficient for electrical resistivity · Materials with heterogenous conductivity	· Addition of a thermally conductive phase · Addition of a conductive phase with low activation energy for electrical conductivity · Decrease of the power peak (step or current rate flash sintering) · Increase furnace temp (tune to material conductivity) · Decrease heating rate or ultrafast (very small time scale)/pulsed · Continuous flash processes (contact or contactless) (variance of current pathway/limited duration of heating) · AC flash (variance of current pathway)
Electrode/center (Electrode region overheated with respect to the center)	High contact resistance between electrodes and sample	· Any	· Use of conductive pastes or pressure to reduce the contact resistance · Electrodes with higher heat capacity · Matching electrode positive temperature coefficient behavior to temperature · Matching AC frequency to charge transfer · Contactless flash sintering
Center/Electrode (Core overheated with respect to the electrode region)	Electrodes act as heatsinks	· Any	· Electrodes with lower heat capacity · Contactless flash sintering
Anode/cathode gradient	Electrochemical redox at DC/low frequency AC	· More evident in ionic conductors	· AC flash sintering · Use of nonblocking electrodes · Reintroduce lost ionic species (atmosphere/molten salt)

homogeneity through the use of insulation has been attempted by researchers developing a flash-SPS hybrid.<sup>90</sup> Similar effects may be applicable to microwave sintering or microwave flash, which can display a similar thermal runaway mechanism.<sup>67</sup> Future efforts should explore both engineering solutions for insulation and alternate creative technical approaches.

## Acknowledgments

The authors thank D. Pearmain of Lucideon Ltd. for helpful discussions and support. Funding for the PhD RD&I Associate for G.M.J. was provided from Lucideon Ltd. and the European Regional Development Fund as part of the “Smart Energy Network Demonstrator” based at Keele University (Grant Reference 32R16P00706). C.E.J.D. acknowledges funding from the Engineering and Physical Sciences Research Council (EP/R029873/1).

## References

1. C.E.J. Dancer, *Mater. Res. Express* **3**, 102001 (2016)
2. M. Yu, S. Grasso, R. McKinnon, T. Saunders, M.J. Reece, *Adv. Appl. Ceram.* **116**, 24 (2017)
3. M. Biesuz, V.M. Sglavo, *J. Eur. Ceram. Soc.* **39**, 115 (2019)
4. R.I. Todd, E. Zapata-Solvas, R.S. Bonilla, T. Sneddon, P.R. Wilshaw, *J. Eur. Ceram. Soc.* **35**, 1865 (2015)
5. Y. Zhang, J. Jung, J. Luo, *Acta Mater.* **94**, 87 (2015)
6. E. Zapata-Solvas, D. Gómez-García, A. Domínguez-Rodríguez, R.I. Todd, *Sci. Rep.* **5**, 1 (2015)
7. S. Grasso, T. Saunders, H. Porwal, B. Milsom, A. Tudball, M. Reece, I.W. Chen, *J. Am. Ceram. Soc.* **99**, 1534 (2016)
8. C. Manière, G. Lee, E.A. Olevsky, *Sci. Rep.* **7**, 1 (2017)
9. Y.V. Bykov, S.V. Egorov, A.G. Ereemeev, V.V. Kholoptsev, I.V. Plotnikov, K.I. Rybakov, A.A. Sorokin, *Materials* **9**, 1 (2016)
10. C. Manière, G. Lee, T. Zahrah, E.A. Olevsky, *Acta Mater.* **147**, 24 (2018)



11. M. Biesuz, V.M. Sglavo, *Scr. Mater.* **187**, 49 (2020)
12. A. Kumar, G. Sharma, A. Aftab, M.I. Ahmad, *J. Eur. Ceram. Soc.* **40**, 3358 (2020)
13. J. Xia, K. Ren, Y. Wang, *Scr. Mater.* **165**, 34 (2019)
14. P. Tatarko, S. Grasso, T.G. Saunders, V. Casalegno, M. Ferraris, M.J. Reece, *J. Eur. Ceram. Soc.* **37**, 3841 (2017)
15. J. Xia, K. Ren, Y. Wang, L. An, *Scr. Mater.* **153**, 31 (2018)
16. C. McLaren, W. Heffner, R. Tessarollo, R. Raj, H. Jain, *Appl. Phys. Lett.* **107**, 1 (2015)
17. H. Yoshida, Y. Sasaki, *Scr. Mater.* **146**, 173 (2018)
18. L.A. Perez-Maqueda, E. Gil-Gonzalez, A. Perejon, J.-M. Lebrun, P. Sanchez-Jimenez, R. Raj, *J. Am. Ceram. Soc.* **100**, 3365 (2017)
19. M. Yu, T. Saunders, S. Grasso, A. Mahajan, H. Zhang, M.J. Reece, *Scr. Mater.* **146**, 241 (2018)
20. T.P. Mishra, R.R.I. Neto, G. Speranza, A. Quaranta, V.M. Sglavo, R. Raj, O. Guillon, M. Bram, M. Biesuz, *Scr. Mater.* **179**, 55 (2020)
21. M. Jongmanns, D.E. Wolf, *J. Am. Ceram. Soc.* **103**, 589 (2020)
22. S. Marinell, E. Savary, M. Gomina, *J. Microw. Power Electromagn. Energy* **44**, 57 (2010)
23. M. Biesuz, L. Pinter, T. Saunders, M. Reece, J. Binner, V.M. Sglavo, S. Grasso, *Materials* **11**, 1214 (2018)
24. G. Liu, D. Liu, J. Liu, Y. Gao, Y. Wang, *J. Eur. Ceram. Soc.* **38**, 2893 (2018)
25. M. Cesar Steil, D. Marinha, Y. Aman, J.R.C. Gomes, M. Kleitz, *J. Eur. Ceram. Soc.* **33**, 2093 (2013)
26. J. Lebrun, S.K. Jha, S.J. McCormack, W.M. Kriven, R. Raj, *J. Am. Ceram. Soc.* **99**, 3429 (2016)
27. J.V. Campos, I.R. Lavagnini, J.G.P. da Silva, J.A. Ferreira, R.V. Sousa, R. Mücke, O. Guillon, E.M.J.A. Pallone, *Scr. Mater.* **186**, 1 (2020)
28. M. Biesuz, M. Cipriani, V.M. Sglavo, G.D. Sorarù, *Scr. Mater.* **182**, 94 (2020)
29. Y.V. Bykov, S.V. Egorov, A.G. Ereemeev, I.V. Plotnikov, K.I. Rybakov, A.A. Sorokin, V.V. Kholoptsev, *Tech. Phys.* **63**, 391 (2018)
30. T.B. Holland, U. Anselmi-Tamburini, D.V. Quach, T.B. Tran, A.K. Mukherjee, *J. Eur. Ceram. Soc.* **32**, 3667 (2012)
31. Y. Michiyuki, S. Falco, R.I. Todd, *J. Ceram. Soc. Jpn.* **126**, 579 (2018)
32. R. Serrazina, P.M. Vilarinho, A.M.O.R. Senos, L. Pereira, I.M. Reaney, J.S. Dean, *J. Eur. Ceram. Soc.* **40**, 1205 (2020)
33. R. Chaim, *Materials* **10**, 179 (2017)
34. J. Narayan, *Scr. Mater.* **68**, 785 (2013)
35. K.S.N. Vikrant, H. Wang, A. Jana, H. Wang, R.E. Garcia, *NPJ Comput. Mater.* **6**, 98 (2020)
36. Y. Dong, *Condens. Mater. Sci.* (2017), <https://arXiv.org/abs/1702.05565>.
37. R. Chaim, C. Estournès, *J. Mater. Sci.* **53**, 6378 (2018)
38. W. Qin, H. Majidi, J. Yun, K. van Benthem, *J. Am. Ceram. Soc.* **99**, 2253 (2016)
39. M. Cologna, B. Rashkova, R. Raj, *J. Am. Ceram. Soc.* **93**, 3556 (2010)
40. M. Cologna, A.L.G. Prette, R. Raj, *J. Am. Ceram. Soc.* **94**, 316 (2011)
41. M.K. Punith Kumar, D. Yadav, J.M. Lebrun, R. Raj, *J. Am. Ceram. Soc.* **102**, 823 (2018)
42. B. Yoon, D. Yadav, S. Ghose, P. Sarin, R. Raj, *J. Am. Ceram. Soc.* **102**, 3110 (2019)
43. H. Charalambous, S.K. Jha, J. Okasinski, T. Tsakalakos, *Materialia* **6**, 100273 (2019)
44. R. Muccillo, M. Kleitz, E.N.S. Muccillo, *J. Eur. Ceram. Soc.* **31**, 1517 (2011)
45. Y. Zhang, J. Nie, J. Luo, *J. Ceram. Soc. Jpn.* **124**, 296 (2016)
46. J. Nie, Y. Zhang, J.M. Chan, S. Jiang, R. Huang, J. Luo, *Scr. Mater.* **141**, 6 (2017)
47. S. Grasso, E.Y. Kim, T. Saunders, M. Yu, A. Tudball, S.H. Choi, M. Reece, *Cryst. Growth Des.* **16**, 2317 (2016)
48. S. Grasso, T. Saunders, H. Porwal, O. Cedillos-Barraza, D.D. Jayaseelan, W.E. Lee, M.J. Reece, *J. Am. Ceram. Soc.* **97**, 2405 (2014)
49. R. McKinnon, S. Grasso, A. Tudball, M.J. Reece, *J. Eur. Ceram. Soc.* **37**, 2787 (2017)
50. D. Demirskyi, O. Vasylyuk, *J. Alloys Compd.* **691**, 466 (2017)
51. B. Dargatz, J. Gonzalez-Julian, M. Bram, Y. Shinoda, F. Wakai, O. Guillon, *J. Eur. Ceram. Soc.* **36**, 1221 (2016)
52. S.K. Jha, R. Raj, *J. Am. Ceram. Soc.* **97**, 3103 (2014)
53. K.S. Naik, V.M. Sglavo, R. Raj, *J. Eur. Ceram. Soc.* **34**, 2435 (2014)
54. V. Avila, R. Raj, *J. Am. Ceram. Soc.* **102**, 6443 (2019)
55. M. Biesuz, W.D. Abate, V.M. Sglavo, *J. Am. Ceram. Soc.* **101**, 71 (2018)
56. J.S.C. Francis, M. Cologna, R. Raj, *J. Eur. Ceram. Soc.* **32**, 3129 (2012)
57. L. Pinter, M. Biesuz, V.M. Sglavo, T. Saunders, J. Binner, M. Reece, S. Grasso, *Scr. Mater.* **151**, 14 (2018)
58. C.T. McLaren, C. Kopatz, N.J. Smith, H. Jain, *Sci. Rep.* **9**, 2805 (2019)
59. C.A. Grimley, A.L.G. Prette, E.C. Dickey, *Acta Mater.* **174**, 271 (2019)
60. S.K. Jha, H. Charalambous, H. Wang, X.L. Phuah, C. Mead, J. Okasinski, H. Wang, T. Tsakalakos, *Ceram. Int.* **44**, 15362 (2018)
61. T.P. Mishra, A.M. Laptev, M. Ziegner, S.K. Sistla, A. Kaletsch, C. Broeckmann, O. Guillon, M. Bram, *Materials* **13**, 3184 (2020)
62. J. Janek, C. Korte, *Solid State Ionics* **116**, 181 (1999)
63. S.W. Kim, S.G. Kim, J. Jung, S.J.L. Kang, I.W. Chen, *J. Am. Ceram. Soc.* **94**, 4231 (2011)
64. V. Esposito, D.W. Ni, D. Marani, F. Teocoli, T. Sune, D.Z. De Florio, F.C. Fonseca, *J. Mater. Chem. A* **4**, 16871 (2016)
65. W. Ji, J. Zhang, W. Wang, Z. Fu, R. Todd, *J. Eur. Ceram. Soc.* **40**, 5829 (2020)
66. W. Ji, B. Parker, S. Falco, J.Y. Zhang, Z.Y. Fu, R.I. Todd, *J. Eur. Ceram. Soc.* **37**, 2547 (2017)
67. C. Manière, F. Borie, S. Marinell, *J. Manuf. Proc.* **56**, 147 (2020)
68. S.V. Egorov, K.I. Rybakov, V.E. Semenov, Y.V. Bykov, O.N. Kanygina, E.B. Kulumbaev, V.M. Lelevkin, *J. Mater. Sci.* **42**, 2097 (2007)
69. M. Biesuz, J. Dong, S. Fu, Y. Liu, H. Zhang, D. Zhu, C. Hu, S. Grasso, *Scr. Mater.* **162**, 99 (2019)
70. M. Oghbaei, O. Mirzaee, *J. Alloys Compd.* **494**, 175 (2010)
71. F. Lemke, W. Rheinheimer, M.J. Hoffmann, *Scr. Mater.* **130**, 187 (2017)
72. H. Charalambous, S.K. Jha, K.H. Christian, R.T. Lay, T. Tsakalakos, *J. Eur. Ceram. Soc.* **38**, 3689 (2018)
73. K.H. Christian, H. Charalambous, S.K. Jha, T. Tsakalakos, *J. Eur. Ceram. Soc.* **40**, 436 (2020)
74. J.V. Campos, I.R. Lavagnini, R.V. de Sousa, J.A. Ferreira, E.M.J.A. Pallone, *J. Eur. Ceram. Soc.* **39**, 531 (2019)
75. I.R. Lavagnini, J.V. Campos, J.A. Ferreira, E.M.J. Eliria, *J. Am. Ceram. Soc.* **103**, 3493 (2020)
76. Lucideon, "Flash Sintering - Technology Scale-up for Advanced Manufacturing" Data Sheet (2020), <https://www.lucideon.com/materials-technologies/flash-sintering>.
77. C.T. McLaren, W.R. Heffner, R. Raj, H. Jain, *J. Am. Ceram. Soc.* **101**, 2277 (2018)
78. A. Eqbal, K.S. Arya, T. Chakrabarti, *Ceram. Int.* **46**, 10370 (2020)
79. X. Li, R. Huang, X. Wang, G. Liu, Z. Jia, L. Wang, *Scr. Mater.* **186**, 158 (2020)
80. E. Sortino, J.M. Lebrun, A. Sansone, R. Raj, *J. Am. Ceram. Soc.* **101**, 1432 (2018)
81. T. Saunders, S. Grasso, M.J. Reece, *Sci. Rep.* **6**, 27222 (2016)
82. S.L. Johnson, G. Venugopal, A.T. Hunt, *J. Am. Ceram. Soc.* **101**, 536 (2018)
83. J. Dong, Z. Wang, X. Zhao, M. Biesuz, T. Saunders, Z. Zhang, C. Hu, S. Grasso, *Scr. Mater.* **175**, 20 (2020)
84. R. Muccillo, A.S. Ferlauto, E.N.S. Muccillo, *Ceramics* **2**, 64 (2019)
85. G. Fele, M. Biesuz, P. Bettotti, R. Moreno, V.M. Sglavo, *Ceram. Int.* **46**, 23266 (2020)
86. W. Xiao, N. Ni, X. Fan, X. Zhao, Y. Liu, P. Xiao, *J. Mater. Sci. Technol.* **60**, 70 (2021)
87. D. Marinha, M. Belmonte, *J. Eur. Ceram. Soc.* **39**, 389 (2019)
88. L. Guan, J. Li, X. Song, J. Bao, T. Jiang, *Scr. Mater.* **159**, 72 (2019)
89. M. Kermani, M. Biesuz, J. Dong, H. Deng, M. Bortolotti, A. Chiappini, M.J. Reece, V.M. Sglavo, C. Hu, S. Grasso, *J. Eur. Ceram. Soc.* **40**, 6266 (2020)
90. M. Bram, A.M. Laptev, T.P. Mishra, K. Nur, M. Kindelmann, M. Ihrig, J.G. Pereira da Silva, R. Steinert, H.P. Buchkremer, A. Litnovsky, F. Klein, J. Gonzalez-Julian, O. Guillon, *Adv. Eng. Mater.* **22**, 2000051 (2020) □